Search for $B^+ \to K^+ \nu\bar{\nu}$ Decays Using an Inclusive Tagging Method at Belle II

F. Abudinén,[44] I. Adachi,[21,19] K. Adamczyk,[66] P. Ahlburg,[97] H. Aihara,[113] N. Akopov,[119] A. Aloisio,[86,37] N. Anh Ky,[34,12] D. M. Asner,[2] H. Atmacan,[99] T. Aushev,[23] V. Aushev,[79] A. Baur,[10] V. Babu,[10] S. Baehr,[48] P. Bambade,[94] Sw. Banerjee,[103] S. Bansal,[72] J. Baudot,[95] J. Becker,[48] P. K. Behera,[27] J. V. Bennett,[107] E. Bernieri,[42] F. U. Bernlochner,[97] M. Bertemes,[30] E. Bertholet,[82] M. Bessner,[101] S. Bettarini,[89,40] F. Bianchi,[91,43] T. Bilka,[6] D. Biswas,[103] A. Bozek,[66] M. Bračko,[105,78] P. Branchini,[42] N. Braun,[48] T. E. Browder,[101] A. Budano,[42] S. Bussino,[90,42] M. Campajola,[86,37] L. Cao,[97] G. Casarosa,[89,40] C. Cecchi,[88,39] D. Červenkov,[6] P. Chang,[65] R. Cheaib,[10] V. Chekelian,[59] C. Chen,[49] Y.-T. Chen,[65] B. G. Cheon,[20] K. Chilikin,[54] K. Chirapatpimol,[7] K. Cho,[51] S.-J. Cho,[120] S. Choudhury,[26] D. Cinabro,[117] L. Corona,[89,40] L. M. Cremaldi,[107] S. Cunliffe,[10] T. Czank,[114] F. Dattola,[10] E. De La Cruz-Burelo,[5] G. de Marino,[94] G. De Nardo,[86,37] M. De Nuccio,[10] G. De Pietro,[42] R. de Sangro,[36] M. Destefanis,[91,43] S. Dey,[82] A. De Yta-Hernandez,[5] A. Di Canto,[2] F. Di Capua,[86,37] J. Dingfelder,[97] Z. Doležal,[6] I. Domínguez Jiménez,[85] T. V. Dong,[12] K. Dort,[47] S. Dubey,[101] S. Duell,[97] G. Dujany,[95] S. Eidelman,[3,54,68] M. Eliachevitch,[97] D. Epifanov,[3,68] T. Ferber,[10] D. Ferlewicz,[106] T. Fillinger,[95] G. Finocchiaro,[36] S. Fiore,[41] A. Fodor,[60] F. Forti,[89,40] A. Frey,[17] B. G. Fulsom,[71] N. Gabyshev,[3,68] E. Ganiev,[92,44] M. Garcia-Hernandez,[5] A. Garmash,[3,68] V. Gaur,[116] A. Gaz,[87,38] A. Gellrich,[10] R. Giordano,[86,37] A. Giri,[26] A. Glazov,[10] B. Gobbo,[44] R. Godang,[111] P. Goldenzweig,[48] B. Golob,[102,78] P. Grace,[96] W. Gradl,[46] E. Graziani,[42] D. Greenwald,[81] Y. Guan,[99] K. Gudkova,[3,68] C. Hadjivasiliou,[71] S. Halder,[80] K. Hara,[21,19] O. Hartbrich,[101] K. Hayasaka,[67] H. Hayashii,[64] S. Hazra,[80] C. Hearty,[98,33] I. Heredia de la Cruz,[5,9] M. Hernández Villanueva,[107] A. Hershenhorn,[98] T. Higuchi,[114] E. C. Hill,[98] H. Hirata,[62] M. Hoek,[46] M. Hohmann,[106] C.-L. Hsu,[112] T. Humair,[59] T. Iijima,[62,63] K. Inami,[62] G. Inguglia,[30] J. Irakkathil Jabbar,[48] A. Ishikawa,[21,19] R. Itoh,[21,19] M. Iwasaki,[69] Y. Iwasaki,[21] P. Jackson,[96] W. W. Jacobs,[28] D. E. Jaffe,[2] Y. Jin,[44] C. Joo,[114] H. Junkerkalefeld,[97] A. B. Kaliyar,[80] J. Kandra,[6] K. H. Kang,[53] R. Karl,[10] G. Karyan,[119] T. Kawasaki,[50] C. Ketter,[101] H. Kichimi,[21] C. Kiesling,[59] C.-H. Kim,[20] D. Y. Kim,[77] Y.-K. Kim,[120] T. D. Kimmel,[116] P. Kodyš,[6] T. Koga,[21] S. Kohani,[101] T. Konno,[50] A. Korobov,[3,68] S. Korpar,[105,78] E. Kovalenko,[3,68] T. M. G. Kraetzschmar,[59] F. Krinner,[59] P. Križan,[102,78] P. Krokovny,[3,68] T. Kuhr,[56] J. Kumar,[4] M. Kumar,[58] R. Kumar,[73] K. Kumara,[117] T. Kunigo,[21] S. Kurz,[10] A. Kuzmin,[3,68] Y.-J. Kwon,[120] S. Lacaprara,[38] Y.-T. Lai,[114] C. La Licata,[114] L. Lanceri,[44] J. S. Lange,[47] M. Laurenza,[90,42] K. Lautenbach,[1] F. R. Le Diberder,[94] S. C. Lee,[53] P. Leitl,[59] D. Levit,[81] P. M. Lewis,[97] C. Li,[55] L. K. Li,[99] S. X. Li,[16] Y. B. Li,[16] J. Libby,[27] K. Lieret,[56] Z. Liptak,[31] Q. Y. Liu,[10] D. Liventsev,[117,21] S. Longo,[10] A. Lozar,[78] T. Lueck,[56] C. Lyu,[97] M. Maggiora,[91,43] S. Maity,[25] R. Manfredi,[92,44] E. Manoni,[39] S. Marcello,[91,43] C. Marinas,[35] A. Martini,[10] M. Masuda,[14,70] T. Matsuda,[108] K. Matsuoka,[21] D. Matvienko,[3,54,68] F. Meier,[11] M. Merola,[86,37] F. Metzner,[48] M. Milesi,[106] C. Miller,[115] K. Miyabayashi,[64] H. Miyake,[21,19] R. Mizuk,[54,23] G. B. Mohanty,[80] H.-G. Moser,[59] M. Mrvar,[30] F. J. Müller,[10] C. Murphy,[114] R. Mussa,[43] K. R. Nakamura,[21,19] M. Nakao,[21,19] Z. Natkaniec,[66] A. Natochii,[101] M. Nayak,[82] G. Nazaryan,[119] C. Niebuhr,[10] N. K. Nisar,[2] S. Nishida,[21,19] K. Nishimura,[101] S. Ogawa,[83] Y. Onishchuk,[79] H. Ono,[67] Y. Onuki,[113] P. Oskin,[54] H. Ozaki,[21,19] P. Pakhlov,[54,61] G. Pakhlova,[23,54] A. Paladino,[89,40] T. Pang,[109] A. Panta,[107] E. Paoloni,[89,40] S. Pardi,[37] H. Park,[53] S.-H. Park,[21] B. Paschen,[97] A. Passeri,[42] A. Pathak,[103] S. Patra,[24] S. Paul,[81] T. K. Pedlar,[57] I. Peruzzi,[36] R. Pestotnik,[78] M. Piccolo,[36] L. E. Piilonen,[116] P. L. M. Podesta-Lerma,[85] T. Podobnik,[78] S. Pokharel,[107] G. Polat,[1] V. Popov,[23] C. Praz,[10] S. Prell,[49] E. Prencipe,[15] M. T. Prim,[97] N. Rad,[10] P. Rados,[10] S. Raiz,[92,44] M. Remnev,[3,68] I. Ripp-Baudot,[95] M. Ritter,[56] G. Rizzo,[89,40] L. B. Rizzuto,[78] S. H. Robertson,[60,33] D. Rodríguez Pérez,[85] J. M. Roney,[115,33] A. Rostomyan,[10] N. Rout,[27] G. Russo,[86,37] D. Sahoo,[80] D. A. Sanders,[107] S. Sandilya,[26] A. Sangal,[99] L. Santelj,[102,78] Y. Sato,[21] V. Savinov,[109] B. Scavino,[46] J. Schueler,[101] C. Schwanda,[30] A. J. Schwartz,[99] R. M. Seddon,[60] Y. Seino,[67] A. Selce,[42,13] K. Senyo,[118] J. Serrano,[1] M. E. Sevior,[106] C. Sfienti,[46] J.-G. Shiu,[65] B. Shwartz,[3,68] A. Sibidanov,[101] F. Simon,[59] R. J. Sobie,[115,33] A. Soffer,[82] A. Sokolov,[29] E. Solovieva,[54] S. Spataro,[91,43] B. Spruck,[46] M. Starič,[78] S. Stefkova,[10] Z. S. Stottler,[116] R. Stroili,[87,38] M. Sumihama,[18,70] K. Sumisawa,[21,19] D. J. Summers,[107,*] W. Sutcliffe,[97] S. Y. Suzuki,[21,19] H. Svidras,[10] M. Tabata,[8] M. Takahashi,[10] M. Takizawa,[74,22,75] U. Tamponi,[43] S. Tanaka,[21,19] K. Tanida,[45] H. Tanigawa,[113] N. Taniguchi,[21] P. Taras,[93] F. Tenchini,[10] D. Tonelli,[44] E. Torassa,[38] N. Toutounji,[112] K. Trabelsi,[94] M. Uchida,[84] Y. Unno,[20] K. Uno,[67] S. Uno,[21,19] P. Urquijo,[106] Y. Ushiroda,[21,19,113] Y. V. Usov,[3,68] S. E. Vahsen,[101] R. van Tonder,[97] G. S. Varner,[101] K. E. Varvell,[112] A. Vinokurova,[3,68] L. Vitale,[92,44] B. Wach,[59] E. Waheed,[21] H. M. Wakeling,[60] W. Wan Abdullah,[104] M.-Z. Wang,[65] X. L. Wang,[16] A. Warburton,[60] S. Watanuki,[94] J. Webb,[106] M. Welsch,[97] C. Wessel,[97] J. Wiechczynski,[40] H. Windel,[59] X. P. Xu,[76] B. D. Yabsley,[112] S. Yamada,[21] W. Yan,[110] S. B. Yang,[52] H. Ye,[10] J. Yelton,[100] J. H. Yin,[52] Y. M. Yook,[32] K. Yoshihara,[62] C. Z. Yuan,[32] Y. Yusa,[67] L. Zani,[1] V. Zhilich,[3,68] Q. D. Zhou,[62,121,63] X. Y. Zhou,[55] and V. I. Zhukova[54]

(Belle II Collaboration)

[1]Aix Marseille Université, CNRS/IN2P3, CPPM, 13288 Marseille
[2]Brookhaven National Laboratory, Upton, New York 11973
[3]Budker Institute of Nuclear Physics SB RAS, Novosibirsk 630090
[4]Carnegie Mellon University, Pittsburgh, Pennsylvania 15213
[5]Centro de Investigacion y de Estudios Avanzados del Instituto Politecnico Nacional, Mexico City 07360
[6]Faculty of Mathematics and Physics, Charles University, 121 16 Prague
[7]Chiang Mai University, Chiang Mai 50202, Thailand
[8]Chiba University, Chiba 263-8522
[9]Consejo Nacional de Ciencia y Tecnología, Mexico City 03940
[10]Deutsches Elektronen–Synchrotron, 22607 Hamburg
[11]Duke University, Durham, North Carolina 27708
[12]Institute of Theoretical and Applied Research (ITAR), Duy Tan University, Hanoi 100000
[13]ENEA Casaccia, I-00123 Roma
[14]Earthquake Research Institute, University of Tokyo, Tokyo 113-0032
[15]Forschungszentrum Jülich, 52425 Jülich
[16]Key Laboratory of Nuclear Physics and Ion-beam Application (MOE) and Institute of Modern Physics, Fudan University, Shanghai 200443
[17]II. Physikalisches Institut, Georg-August-Universität Göttingen, 37073 Göttingen
[18]Gifu University, Gifu 501-1193
[19]The Graduate University for Advanced Studies (SOKENDAI), Hayama 240-0193
[20]Department of Physics and Institute of Natural Sciences, Hanyang University, Seoul 04763
[21]High Energy Accelerator Research Organization (KEK), Tsukuba 305-0801
[22]J-PARC Branch, KEK Theory Center, High Energy Accelerator Research Organization (KEK), Tsukuba 305-0801
[23]National Research University Higher School of Economics, Moscow 101000
[24]Indian Institute of Science Education and Research Mohali, SAS Nagar, 140306
[25]Indian Institute of Technology Bhubaneswar, Satya Nagar 751007
[26]Indian Institute of Technology Hyderabad, Telangana 502285
[27]Indian Institute of Technology Madras, Chennai 600036
[28]Indiana University, Bloomington, Indiana 47408
[29]Institute for High Energy Physics, Protvino 142281
[30]Institute of High Energy Physics, Vienna 1050
[31]Hiroshima University, Higashi-Hiroshima, Hiroshima 739-8530
[32]Institute of High Energy Physics, Chinese Academy of Sciences, Beijing 100049
[33]Institute of Particle Physics (Canada), Victoria, British Columbia V8W 2Y2
[34]Institute of Physics, Vietnam Academy of Science and Technology (VAST), Hanoi
[35]Instituto de Fisica Corpuscular, Paterna 46980
[36]INFN Laboratori Nazionali di Frascati, I-00044 Frascati
[37]INFN Sezione di Napoli, I-80126 Napoli
[38]INFN Sezione di Padova, I-35131 Padova
[39]INFN Sezione di Perugia, I-06123 Perugia
[40]INFN Sezione di Pisa, I-56127 Pisa
[41]INFN Sezione di Roma, I-00185 Roma
[42]INFN Sezione di Roma Tre, I-00146 Roma
[43]INFN Sezione di Torino, I-10125 Torino
[44]INFN Sezione di Trieste, I-34127 Trieste
[45]Advanced Science Research Center, Japan Atomic Energy Agency, Naka 319-1195
[46]Johannes Gutenberg-Universität Mainz, Institut für Kernphysik, D-55099 Mainz
[47]Justus-Liebig-Universität Gießen, 35392 Gießen
[48]Institut für Experimentelle Teilchenphysik, Karlsruher Institut für Technologie, 76131 Karlsruhe
[49]Iowa State University, Ames, Iowa 50011
[50]Kitasato University, Sagamihara 252-0373
[51]Korea Institute of Science and Technology Information, Daejeon 34141
[52]Korea University, Seoul 02841
[53]Kyungpook National University, Daegu 41566
[54]P. N. Lebedev Physical Institute of the Russian Academy of Sciences, Moscow 119991
[55]Liaoning Normal University, Dalian 116029
[56]Ludwig Maximilians University, 80539 Munich

[57]Luther College, Decorah, Iowa 52101
[58]Malaviya National Institute of Technology Jaipur, Jaipur 302017
[59]Max-Planck-Institut für Physik, 80805 München
[60]McGill University, Montréal, Québec, H3A 2T8
[61]Moscow Physical Engineering Institute, Moscow 115409
[62]Graduate School of Science, Nagoya University, Nagoya 464-8602
[63]Kobayashi-Maskawa Institute, Nagoya University, Nagoya 464-8602
[64]Nara Women's University, Nara 630-8506
[65]Department of Physics, National Taiwan University, Taipei 10617
[66]H. Niewodniczanski Institute of Nuclear Physics, Krakow 31-342
[67]Niigata University, Niigata 950-2181
[68]Novosibirsk State University, Novosibirsk 630090
[69]Osaka City University, Osaka 558-8585
[70]Research Center for Nuclear Physics, Osaka University, Osaka 567-0047
[71]Pacific Northwest National Laboratory, Richland, Washington 99352
[72]Panjab University, Chandigarh 160014
[73]Punjab Agricultural University, Ludhiana 141004
[74]Meson Science Laboratory, Cluster for Pioneering Research, RIKEN, Saitama 351-0198
[75]Showa Pharmaceutical University, Tokyo 194-8543
[76]Soochow University, Suzhou 215006
[77]Soongsil University, Seoul 06978
[78]J. Stefan Institute, 1000 Ljubljana
[79]Taras Shevchenko National University of Kiev, Kiev
[80]Tata Institute of Fundamental Research, Mumbai 400005
[81]Department of Physics, Technische Universität München, 85748 Garching
[82]School of Physics and Astronomy, Tel Aviv University, Tel Aviv, 69978
[83]Toho University, Funabashi 274-8510
[84]Tokyo Institute of Technology, Tokyo 152-8550
[85]Universidad Autonoma de Sinaloa, Sinaloa 80000
[86]Dipartimento di Scienze Fisiche, Università di Napoli Federico II, I-80126 Napoli
[87]Dipartimento di Fisica e Astronomia, Università di Padova, I-35131 Padova
[88]Dipartimento di Fisica, Università di Perugia, I-06123 Perugia
[89]Dipartimento di Fisica, Università di Pisa, I-56127 Pisa
[90]Dipartimento di Matematica e Fisica, Università di Roma Tre, I-00146 Roma
[91]Dipartimento di Fisica, Università di Torino, I-10125 Torino
[92]Dipartimento di Fisica, Università di Trieste, I-34127 Trieste
[93]Université de Montréal, Physique des Particules, Montréal, Québec, H3C 3J7
[94]Université Paris-Saclay, CNRS/IN2P3, IJCLab, 91405 Orsay
[95]Université de Strasbourg, CNRS, IPHC, UMR 7178, 67037 Strasbourg
[96]Department of Physics, University of Adelaide, Adelaide, South Australia 5005
[97]University of Bonn, 53115 Bonn
[98]University of British Columbia, Vancouver, British Columbia, V6T 1Z1
[99]University of Cincinnati, Cincinnati, Ohio 45221
[100]University of Florida, Gainesville, Florida 32611
[101]University of Hawaii, Honolulu, Hawaii 96822
[102]Faculty of Mathematics and Physics, University of Ljubljana, 1000 Ljubljana
[103]University of Louisville, Louisville, Kentucky 40292
[104]National Centre for Particle Physics, University Malaya, 50603 Kuala Lumpur
[105]Faculty of Chemistry and Chemical Engineering, University of Maribor, 2000 Maribor
[106]School of Physics, University of Melbourne, Victoria 3010
[107]University of Mississippi, University, Mississippi 38677
[108]University of Miyazaki, Miyazaki 889-2192
[109]University of Pittsburgh, Pittsburgh, Pennsylvania 15260
[110]University of Science and Technology of China, Hefei 230026
[111]University of South Alabama, Mobile, Alabama 36688
[112]School of Physics, University of Sydney, New South Wales 2006
[113]Department of Physics, University of Tokyo, Tokyo 113-0033
[114]Kavli Institute for the Physics and Mathematics of the Universe (WPI), University of Tokyo, Kashiwa 277-8583
[115]University of Victoria, Victoria, British Columbia, V8W 3P6
[116]Virginia Polytechnic Institute and State University, Blacksburg, Virginia 24061

[117]Wayne State University, Detroit, Michigan 48202
[118]Yamagata University, Yamagata 990-8560
[119]Alikhanyan National Science Laboratory, Yerevan 0036
[120]Yonsei University, Seoul 03722
[121]Institute for Advanced Research, Nagoya University, Nagoya 464-8602

(Received 6 May 2021; revised 23 July 2021; accepted 10 September 2021; published 27 October 2021)

A search for the flavor-changing neutral-current decay $B^+ \to K^+\nu\bar{\nu}$ is performed at the Belle II experiment at the SuperKEKB asymmetric energy electron-positron collider. The data sample corresponds to an integrated luminosity of 63 fb^{-1} collected at the $\Upsilon(4S)$ resonance and a sample of 9 fb^{-1} collected at an energy 60 MeV below the resonance. Because the measurable decay signature involves only a single charged kaon, a novel measurement approach is used that exploits not only the properties of the $B^+ \to K^+\nu\bar{\nu}$ decay, but also the inclusive properties of the other B meson in the $\Upsilon(4S) \to B\bar{B}$ event, to suppress the background from other B meson decays and light-quark pair production. This inclusive tagging approach offers a higher signal efficiency compared to previous searches. No significant signal is observed. An upper limit on the branching fraction of $B^+ \to K^+\nu\bar{\nu}$ of 4.1×10^{-5} is set at the 90% confidence level.

DOI: 10.1103/PhysRevLett.127.181802

Flavor-changing neutral-current transitions, such as $b \to s\nu\bar{\nu}$, are suppressed in the standard model (SM) by the extended Glashow-Iliopoulos-Maiani mechanism [1]. These transitions can only occur at higher orders in SM perturbation theory via weak amplitudes involving the exchange of at least two gauge bosons, as illustrated in Fig. 1. The absence of charged leptons in the final state reduces the theoretical uncertainty compared to similar $b \to s\ell\ell$ transitions, which are affected by the breakdown of factorization due to photon exchange [2]. The branching fraction of the $B^+ \to K^+\nu\bar{\nu}$ decay [3], which involves a $b \to s\nu\bar{\nu}$ transition, is predicted to be $(4.6 \pm 0.5) \times 10^{-6}$, where the main contribution to the uncertainty arises from the $B^+ \to K^+$ transition form factor [4].

Studies of this rare decay are currently of particular interest, as this process offers a complementary probe of potential non-SM physics scenarios that are proposed to explain the tensions with the SM predictions in $b \to s\ell^+\ell^-$ transitions [5] observed in Refs. [6–11]. More generally, measurements of the $B^+ \to K^+\nu\bar{\nu}$ decay help constrain models that predict new particles, such as leptoquarks [12], axions [13], or dark matter particles [14].

The study of the $B^+ \to K^+\nu\bar{\nu}$ decay is experimentally challenging as the final state contains two neutrinos, which leave no signature in the detector and cannot be used to derive information about the signal B meson. Previous searches used *tagged* approaches, where the second B meson produced in the $e^+e^- \to \Upsilon(4S) \to B\bar{B}$ event is explicitly reconstructed in a hadronic decay [15–17] or in a semileptonic decay [18,19]. This tagging suppresses background events but results in a low signal reconstruction efficiency, typically well below 1%. In all analyses reported to date, no evidence for a signal is found, and the current experimental upper limit on the branching fraction is estimated to be 1.6×10^{-5} at 90% confidence level [20].

In this search, a novel and independent *inclusive* tagging approach is used, inspired by Ref. [21]. This approach has the benefit of a larger signal efficiency of about 4%, at the cost of higher background levels. The method exploits the distinctive topological and kinematic features of the $B^+ \to K^+\nu\bar{\nu}$ decay that distinguish this process from the seven dominant background categories. These are other decays of charged B mesons, decays of neutral B mesons, and the five continuum categories $e^+e^- \to q\bar{q}$ with $q = u,\ d,\ s,\ c$ quarks and $e^+e^- \to \tau^+\tau^-$. The signal candidates are reconstructed as a single charged-particle trajectory (track) generated by the kaon, typically carrying higher momentum than background particles. The remaining tracks and energy deposits, referred to as the "rest of the event" (ROE), can thus be associated with the decay of the accompanying B meson. Furthermore, the neutrinos produced in the signal B meson decay typically carry a significant fraction of its energy. The resulting "missing momentum" is defined as the momentum needed to cancel

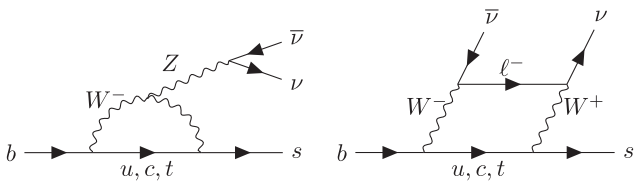

(a) Penguin diagram (b) Box diagram

FIG. 1. The lowest-order quark-level diagrams for the $b \to s\nu\bar{\nu}$ transition in the SM are either of the penguin (a) or the box (b) type.

the sum of the three-momenta of all reconstructed tracks and energy deposits in the center-of-mass system of the incoming beams. The specific properties of signal events are captured in a variety of discriminating variables used as inputs for event classifiers to separate signal from background.

This search uses data from e^+e^- collisions produced in 2019 and 2020 by the SuperKEKB collider [22]. The data, corresponding to an integrated luminosity of 63 fb^{-1} [23], were recorded by the Belle II detector at a center-of-mass energy of $\sqrt{s} = 10.58$ GeV, which corresponds to the $\Upsilon(4S)$ resonance, and contain 68 million $B\bar{B}$ pairs [24]. An additional off-resonance sample of 9 fb^{-1} integrated luminosity, collected at an energy 60 MeV lower than the $\Upsilon(4S)$ resonance, is used to constrain the yields of continuum events.

The signal and background samples are generated using a variety of event generators, summarized in the Supplemental Material [25], with the detector response simulated by the Belle II Analysis Software Framework (BASF2) [31], interfaced with GEANT4 [32]. The simulated $B^+ \to K^+\nu\bar{\nu}$ events are weighted according to the SM form-factor calculations from Ref. [2].

A full description of the Belle II detector is given in Ref. [33]. The detector consists of several subdetectors arranged in a cylindrical structure around the beam pipe. Compared to its predecessor Belle [34], a pixel detector (PXD) has been added at a minimum radius of 1.4 cm. This improves the resolution of the impact parameter to about 12 μm in the transverse direction for high-momentum tracks [35], which helps to reject background events for this analysis. The PXD is surrounded by a four-layer double-sided silicon strip detector, referred to as the silicon vertex detector, and a central drift chamber (CDC). A time-of-propagation counter and an aerogel ring-imaging Cherenkov counter cover the barrel and forward end cap regions of the detector, respectively, and are essential for charged-particle identification (PID). The electromagnetic calorimeter (ECL) makes up the remaining volume inside a superconducting solenoid, which operates at 1.5 T. A dedicated detector to identify K_L^0 mesons and muons is installed in the outermost part of the detector. The z axis of the laboratory frame is defined as the symmetry axis of the solenoid, and the positive direction is approximately given by the incoming electron beam. The polar angle θ, as well as the longitudinal and the transverse direction are defined with respect to the z axis. The relevant online event-selection systems (triggers) for this analysis are based either on the number of tracks in the CDC or on the energy deposits in the calorimeter.

The events are reconstructed using BASF2. The trajectories of charged particles are determined using the algorithms described in Ref. [36]. Charged particles are required to have a transverse momentum $p_T > 0.1$ GeV/c, to be within the CDC acceptance ($17° < \theta < 150°$), and to have longitudinal and transverse impact parameters with respect to the average interaction point of $|d_z| < 3$ and $d_r < 0.5$ cm, respectively. Photons are identified as energy deposits in the ECL exceeding 0.1 GeV that are within the CDC acceptance and are not matched to tracks. Each of the charged particles and photons is required to have an energy of less than 5.5 GeV to reject misreconstructed objects and cosmic muons.

Events are required to contain no more than ten reconstructed tracks to suppress background events with only a small loss of signal efficiency. Low track-multiplicity background events are suppressed by demanding at least four tracks in the event. To further suppress such background with a negligible loss of signal events, the total energy from all reconstructed objects in the event must exceed 4 GeV and the polar angle θ of the missing momentum must be between 17° and 160°.

The charged particle with the highest transverse momentum in each event, reconstructed with at least one hit in the PXD, is chosen to be the signal kaon candidate. Studies on simulated signal events show that the chosen candidate is the signal kaon in 78% of the cases. Furthermore, the signal candidate is required to satisfy PID requirements that suppress pion background. The PID requirements retain 62% of kaons while removing 97% of pions for events from the signal region, which is defined below. Simulated events are weighted to correct the dependence of the efficiency of this selection on the transverse momentum and the polar angle of the signal candidate, according to the efficiency observed in data. The remaining charged particles are fit to a common vertex and are attributed, together with the photons, to the ROE.

Simulated signal and background events are used to train binary event classifiers, which are based on the FastBDT algorithm [37], a multivariate method that uses boosted decision trees (BDTs). Several inputs are considered for this process, including general event-shape variables described in Ref. [38], as well as variables characterizing the kaon-candidate and the kinematic properties of the ROE. Moreover, vertices of two and three charged particles, including the kaon candidate, are reconstructed to identify potential kaons from D^0 and D^+ meson decays, and variables describing the fit quality and kinematic properties of the vertices are derived. Variables that are not well described by the simulation and those that do not contribute to the separation power of the classification are removed. This results in a set of 51 training variables, summarized in the Supplemental Material [25].

A first binary classifier BDT_1 is trained on approximately 10^6 simulated events of each of the seven considered background categories and on the same number of signal events. The most discriminating variables are found to be event-shape variables, specifically the reduced Fox-Wolfram moment R_1, which measures the momentum imbalance in the event where the signal tends to be

imbalanced due to signal neutrinos [39], and the modified Fox-Wolfram variables that are functions of the missing momentum and of the momentum of the signal kaon candidate [40].

To improve the training performance at high BDT_1 values, a second classifier BDT_2 is trained with the same set of input variables as BDT_1 on events with $\mathrm{BDT}_1 > 0.9$, which corresponds to a signal efficiency of 28% and a purity of 0.02%. The training is performed using a simulated background sample of 100 fb^{-1} equivalent luminosity (corresponding to a total of 5×10^6 events with $\mathrm{BDT}_1 > 0.9$) and a sample of 1.5×10^6 signal events with $\mathrm{BDT}_1 > 0.9$. An increase of 35% in signal purity is achieved by the additional application of BDT_2 on top of BDT_1, when comparing the performance at a signal efficiency of 4%. BDT_1 and BDT_2 use the same set of FastBDT parameters [37], which are optimized based on a grid search in the parameter space and are specified in the Supplemental Material [25].

An additional binary classifier is used to correct for mismodeling of continuum simulation, following a data-driven method presented in Ref. [41]. More information about the implementation is included in the Supplemental Material [25]. A comparison of simulated continuum events with off-resonance data shows that the application of the derived event weight improves the modeling of all input variables.

A signal region (SR) is defined to be $\mathrm{BDT}_1 > 0.9$ and $\mathrm{BDT}_2 > 0.95$ and is further divided into 3×3 bins in the $\mathrm{BDT}_2 \times p_T(K^+)$ space, where $p_T(K^+)$ is the transverse momentum of the kaon candidate. The bin boundaries, decided by minimizing the expected upper limit on the signal branching fraction, are [0.95, 0.97, 0.99, 1.0] in BDT_2 and $[0.5, 2.0, 2.4, 3.5]$ GeV/c in $p_T(K^+)$. Furthermore, three control regions are used to help constrain the background yields. The control region CR1 consists of 1×3 bins in the $\mathrm{BDT}_2 \times p_T(K^+)$ space, defined at lower values of $\mathrm{BDT}_2 \in [0.93, 0.95]$ and using the same $p_T(K^+)$ bins as the SR. The two other control regions, CR2 and CR3, consist of off-resonance data with identical BDT_2 and $p_T(K^+)$ ranges and bins as in the SR and CR1, respectively.

The expected yields of the SM signal and the backgrounds in the SR are 14 and 844 events, respectively, corresponding to a signal efficiency of 4.3%. In most of these background events, a K^+ produced in a D meson decay is selected as the signal kaon candidate.

To enable the study of other, non-SM signal models, the fraction of signal events in the SR is studied as a function of the generated dineutrino invariant mass squared q^2. The efficiency is 13% for $q^2 = 0$ and drops to zero for $q^2 > 16\ \mathrm{GeV}^2/c^4$. The full distribution can be found in the Supplemental Material [25].

The performance of the classifiers BDT_1 and BDT_2 on data is tested by selecting events with a moderate BDT output of $0.9 < \mathrm{BDT}_1 < 0.99$ and $\mathrm{BDT}_2 < 0.7$ in the $\Upsilon(4S)$ on-resonance data and corresponding simulation. The study confirms the accurate modeling of the BDT distributions by the simulation for a sample of events that have similar kinematic properties as signal events, while containing only a negligible contribution from signal.

The decay $B^+ \to K^+ J/\psi$ with $J/\psi \to \mu^+\mu^-$ is used as an independent validation channel, exploiting its large branching fraction and distinctive experimental signature. These events are selected in data and $B^+ \to K^+ J/\psi$ simulation by requiring the presence of two muons with an invariant mass within 50 MeV/c^2 of the known J/ψ mass [20]. To suppress background events, the variable $|\Delta E| = |E_B^* - \sqrt{s}/2|$ is required to be less than 100 MeV and the beam-energy constrained mass $M_{\mathrm{bc}} = \sqrt{s/(4c^4) - p_B^{*2}/c^2}$ is required to exceed 5.25 GeV/c^2, where E_B^* and p_B^* are given by the energy and the magnitude of the three-momentum of the signal B meson candidate defined in the center-of-mass system of the incoming beams. This results in 1720 events being selected in the data sample at an expected background contamination of 5%. Each event is then reconsidered as a $B^+ \to K^+ \nu\bar{\nu}$ event by ignoring the muons from the J/ψ decay and replacing the momentum of the kaon candidate with the generator-level momentum of the kaon in a randomly selected $B^+ \to K^+ \nu\bar{\nu}$ event from simulation. The same modifications are applied to the data and $B^+ \to K^+ J/\psi$ simulation. The results are summarized in Fig. 2, where the distributions of the output values of both BDTs are shown. Good agreement between simulation and data is observed for the selected events before ($B^+ \to K^+ J/\psi_{\to\mu^+\mu^-}$) and

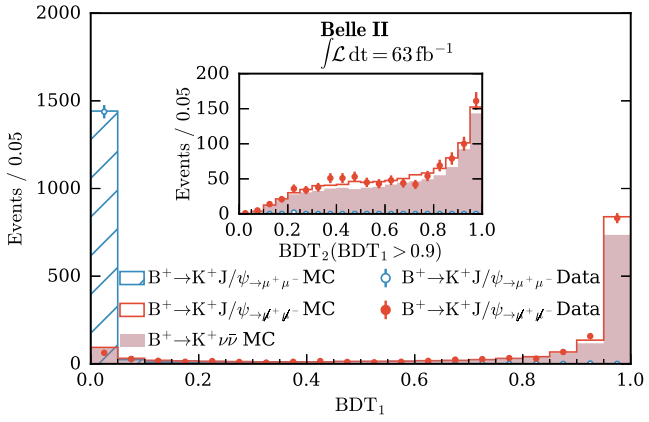

FIG. 2. Distribution of the classifier output BDT_1 (main figure) and BDT_2 for $\mathrm{BDT}_1 > 0.9$ (inset). The distributions are shown before ($J/\psi_{\to\mu^+\mu^-}$) and after ($J/\psi_{\to e^+e^-}$) the muon removal and update of the kaon-candidate momentum of selected $B^+ \to K^+ J/\psi$ events in simulation (MC) and data. As a reference, the classifier outputs directly obtained from simulated $B^+ \to K^+ \nu\bar{\nu}$ signal events are overlaid. The simulation histograms are scaled to the total number of $B^+ \to K^+ J/\psi$ events selected in data.

after ($B^+ \to K^+ J/\psi_{\to \mu^+\mu^-}$) the modifications. The two-sample Kolmogorov-Smirnov p values [42] for the BDT_1 and BDT_2 distributions of simulation and data, after the modifications, are 7% and 23%, respectively. The ratio of the selection efficiencies $\mathrm{BDT}_1 > 0.9$, $\mathrm{BDT}_2 > 0.95$ in data and simulation is found to be 1.06 ± 0.10.

The statistical analysis to determine the signal yields is performed with the PYHF package [43,44], which constructs a binned likelihood following the HISTFACTORY [45] formalism. The templates for the yields of the signal and the seven background categories are derived from simulation. The likelihood function is a product of Poisson probability density functions that combine the information from all 24 signal- and control-region bins defined on the on- and off-resonance data. The systematic uncertainties discussed below are included in the likelihood as nuisance parameters that are event-count modifiers with corresponding constraints modeled as normal probability density functions. The parameter of interest, the signal strength μ, is defined as a factor relative to the SM expectation and is determined simultaneously with the nuisance parameters using a simultaneous maximum-likelihood fit to the binned distribution of data event counts.

The leading systematic uncertainty is the normalization uncertainty on the background yields. The yields of the seven individual background categories are allowed to float independently in the fit. However, each of them is constrained assuming a normal constraint, centered at the expected background yield obtained from simulation and a standard deviation corresponding to 50% of the central value. This value is motivated by a global normalization difference of $(40 \pm 12)\%$ between the off-resonance data and simulation in the control regions CR2 and CR3 and also covers the uncertainty on the sample luminosity. The remaining considered systematic uncertainties may also influence the shape of the templates. Systematic uncertainties originating from the branching fractions of the leading B meson decays, the PID correction, and the SM form factors are accounted for with three nuisance parameters each to model correlations between the individual SR and CR bins. The remaining systematic uncertainties arise from the energy miscalibration of hadronic and beam-background calorimeter energy deposits and the tracking inefficiency, and are each accounted for with one nuisance parameter. The systematic uncertainty due to the limited size of simulated samples is taken into account by one nuisance parameter per bin per background category. This results in a total of 175 nuisance parameters.

To validate the fitting software, an alternative approach based on a simplified Gaussian likelihood function (SGHF) is developed. Tests of both PYHF and SGHF are performed using pseudo-experiments, in which both statistical and systematic uncertainties are taken into account, including background normalizations. No bias in μ and its uncertainty is observed, and the p value for the data and fit model compatibility is found to be above 65%.

Shifts of the nuisance parameters corresponding to the seven background sources are investigated before μ is revealed. The parameters corresponding to the continuum background yields are increased by, at most, one standard deviation, which confirms that they are not pulled substantially in the fit given the observed difference in the normalization of the continuum simulation with respect to the off-resonance data. The background yields in the bins of CR2 and CR3 predicted by the fit are found in agreement with the off-resonance data. No shift is observed for the parameters corresponding to the background yields from charged and neutral B meson decays, which are the dominant contributions in the most sensitive SR bins.

A comparison of the data and fit results in the SR and CR1 is shown in Fig. 3. The corresponding figure for CR2 and CR3 can be found in the Supplemental Material [25]. The signal purity is found to be 6% in the SR and is as high as 22% in the three bins with $\mathrm{BDT}_2 > 0.99$. Continuum events make up 59% of the background in the SR and 28% of the events with $\mathrm{BDT}_2 > 0.99$.

The signal strength is determined by the fit to be $\mu = 4.2^{+3.4}_{-3.2} = 4.2^{+2.9}_{-2.8}(\mathrm{stat})^{+1.8}_{-1.6}(\mathrm{syst})$, where the statistical uncertainty is estimated using pseudo-experiments based on Poisson statistics. The total uncertainty is obtained by a profile likelihood scan, fitting the model with fixed values of μ around the best-fit value, while keeping the other fit parameters free. The systematic uncertainty is calculated by subtracting the statistical uncertainty in quadrature from the total uncertainty. An additional 10% theoretical uncertainty arising from the knowledge of the branching

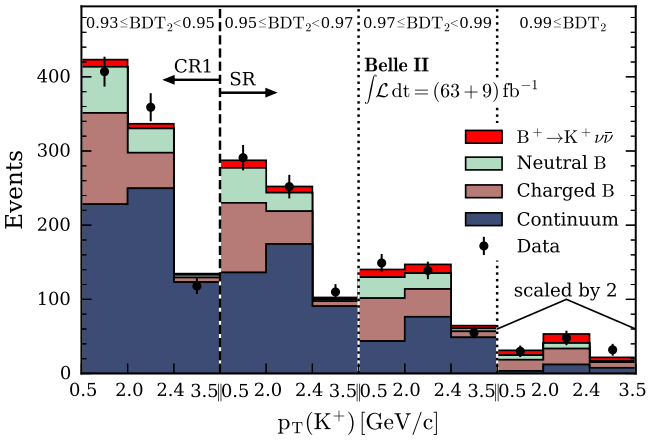

FIG. 3. Yields in on-resonance data and as predicted by the simultaneous fit to the on- and off-resonance data, corresponding to an integrated luminosity of 63 and 9 fb^{-1}, respectively. The predicted yields are shown individually for charged and neutral B meson decays and the sum of the five continuum categories. The leftmost three bins belong to CR1 with $\mathrm{BDT}_2 \in [0.93, 0.95]$ and the other nine bins correspond to the SR, three for each range of $\mathrm{BDT}_2 \in [0.95, 0.97, 0.99, 1.0]$. Each set of three bins is defined by $p_T(K^+) \in [0.5, 2.0, 2.4, 3.5]$ GeV/c. All yields in the rightmost three bins are scaled by a factor of 2.

ratio in the SM is not included. The result corresponds to a branching fraction of the $B^+ \to K^+\nu\bar{\nu}$ decay of $[1.9^{+1.6}_{-1.5}] \times 10^{-5} = [1.9^{+1.3}_{-1.3}(\text{stat})^{+0.8}_{-0.7}(\text{syst})] \times 10^{-5}$.

This value is statistically compatible with the measurements performed by previous experiments. Details are given in the Supplemental Material [25]. The uncertainty on the branching fraction is used to define a measure to compare the performance of the individual tagging techniques. Assuming that this uncertainty scales as the inverse square root of the integrated luminosity [46], the inclusive approach is more than a factor of 3.5 better per integrated luminosity than the hadronic tagging of Ref. [16], approximately 20% better than the semileptonic tagging of Ref. [19], and approximately 10% better than the combined hadronic and semileptonic tagging of Ref. [17]. Moreover, the events in the SR differ from the ones selected by the hadronic and semileptonic tagging so that a statistical combination of the measurements provides additional sensitivity. The inclusive tagging approach can be applied to a variety of decay modes, such as $B^+ \to K^{*+}\nu\bar{\nu}$ and $B^+ \to \tau^+\nu$, and, because of the increased signal efficiency, this can be done on smaller data samples than required for semileptonic or hadronic tagging.

As no significant signal is observed, the expected and observed upper limits on the branching fraction are determined using the CL_s method [47], a modified frequentist approach that is based on a profile likelihood ratio [48]. The expected 90% confidence level (C. L.) upper limit on the $B^+ \to K^+\nu\bar{\nu}$ branching fraction of 2.3×10^{-5} is derived assuming a background-only hypothesis. The observed upper limit is 4.1×10^{-5} at the 90% C.L. The full distribution of the determined CL_s values is shown in the Supplemental Material [25].

In summary, a search for the rare decay $B^+ \to K^+\nu\bar{\nu}$ is performed using an inclusive tagging approach, which has not previously been used to study this process. This analysis uses data corresponding to an integrated luminosity of 63 fb^{-1} collected at the $\Upsilon(4S)$ resonance by the Belle II detector, as well as an off-resonance sample corresponding to 9 fb^{-1}. No statistically significant signal is observed and an upper limit on the branching fraction of 4.1×10^{-5} at the 90% C.L. is set, assuming a SM signal. This measurement is competitive with previous results for similar integrated luminosities, demonstrating the capability of the inclusive tagging approach, which is widely applicable and expands the future physics reach of Belle II.

We thank the SuperKEKB group for the excellent operation of the accelerator; the KEK cryogenics group for the efficient operation of the solenoid; the KEK computer group for on-site computing support; and the raw-data centers at BNL, DESY, GridKa, IN2P3, and INFN for off-site computing support. This work was supported by the following funding sources: Science Committee of the Republic of Armenia Grant No. 20TTCG-1C010; Australian Research Council and research Grants No. DP180102629, No. DP170102389, No. DP170102204, No. DP150103061, No. FT130100303, No. FT130100018, and No. FT120100745; Austrian Federal Ministry of Education, Science and Research, Austrian Science Fund No. P 31361-N36, and Horizon 2020 ERC Starting Grant No. 947006 "InterLeptons"; Natural Sciences and Engineering Research Council of Canada, Compute Canada, and CANARIE; Chinese Academy of Sciences and research Grant No. QYZDJ-SSW-SLH011, National Natural Science Foundation of China and research Grants No. 11521505, No. 11575017, No. 11675166, No. 11761141009, No. 11705209, and No. 11975076, LiaoNing Revitalization Talents Program under Contract No. XLYC1807135, Shanghai Municipal Science and Technology Committee under Contract No. 19ZR1403000, Shanghai Pujiang Program under Grant No. 18PJ1401000, and the CAS Center for Excellence in Particle Physics (CCEPP); the Ministry of Education, Youth, and Sports of the Czech Republic under Contract No. LTT17020 and Charles University Grants No. SVV 260448 and No. GAUK 404316; European Research Council, Seventh Framework PIEF-GA-2013-622527, Horizon 2020 ERC-Advanced Grants No. 267104 and No. 884719, Horizon 2020 ERC-Consolidator Grant No. 819127, Horizon 2020 Marie Sklodowska-Curie Grant Agreement No. 700525 "NIOBE," and Horizon 2020 Marie Sklodowska-Curie RISE project JENNIFER2 Grant Agreement No. 822070 (European grants); L'Institut National de Physique Nucléaire et de Physique des Particules (IN2P3) du CNRS (France); BMBF, DFG, HGF, MPG, and AvH Foundation (Germany); Department of Atomic Energy under Project Identification No. RTI 4002 and Department of Science and Technology (India); Israel Science Foundation Grant No. 2476/17, U.S.-Israel Binational Science Foundation Grant No. 2016113, and Israel Ministry of Science Grant No. 3-16543; Istituto Nazionale di Fisica Nucleare and the research grants BELLE2; Japan Society for the Promotion of Science, Grant-in-Aid for Scientific Research Grants No. 16H03968, No. 16H03993, No. 16H06492, No. 16K05323, No. 17H01133, No. 17H05405, No. 18K03621, No. 18H03710, No. 18H05226, No. 19H00682, No. 26220706, and No. 26400255, the National Institute of Informatics, and Science Information NETwork 5 (SINET5), and the Ministry of Education, Culture, Sports, Science, and Technology (MEXT) of Japan; National Research Foundation (NRF) of Korea Grants No. 2016R1D1A1B01010135, No. 2016R1D1A1B02012900, No. 2018R1A2B3003643, No. 2018R1A6A1A06024970, No. 2018R1D1A1B07047294, No. 2019K1A3A7A09033840, and No. 2019R1I1A3A01058933, Radiation Science Research Institute, Foreign Large-size Research Facility Application Supporting project, the Global Science Experimental Data Hub Center of the

Korea Institute of Science and Technology Information, and KREONET/GLORIAD; Universiti Malaya RU grant, Akademi Sains Malaysia, and Ministry of Education Malaysia; Frontiers of Science Program Contracts No. FOINS-296, No. CB-221329, No. CB-236394, No. CB-254409, and No. CB-180023, and SEP-CINVESTAV research Grant No. 237 (Mexico); the Polish Ministry of Science and Higher Education and the National Science Center; the Ministry of Science and Higher Education of the Russian Federation, Agreement No. 14.W03.31.0026, and the HSE University Basic Research Program, Moscow; University of Tabuk research Grants No. S-0256-1438 and No. S-0280-1439 (Saudi Arabia); Slovenian Research Agency and research Grants No. J1-9124 and No. P1-0135; Agencia Estatal de Investigacion, Spain Grants No. FPA2014-55613-P and No. FPA2017-84445-P, and CIDEGENT/2018/020 of Generalitat Valenciana; Ministry of Science and Technology and research Grants No. MOST106-2112-M-002-005-MY3 and No. MOST107-2119-M-002-035-MY3, and the Ministry of Education (Taiwan); Thailand Center of Excellence in Physics; TUBITAK ULAKBIM (Turkey); Ministry of Education and Science of Ukraine; the U.S. National Science Foundation and research Grants No. PHY-1807007 and No. PHY-1913789, and the U.S. Department of Energy and research Awards No. DE-AC06-76RLO1830, No. DE-SC0007983, No. DE-SC0009824, No. DE-SC0009973, No. DE-SC0010073, No. DE-SC0010118, No. DE-SC0010504, No. DE-SC0011784, No. DE-SC0012704, No. DE-SC0021274; and the Vietnam Academy of Science and Technology (VAST) under Grant No. DL0000.05/21-23.

[*] Deceased.

[1] S. L. Glashow, J. Iliopoulos, and L. Maiani, Phys. Rev. D **2**, 1285 (1970).
[2] A. J. Buras, J. Girrbach-Noe, C. Niehoff, and D. M. Straub, J. High Energy Phys. 02 (2015) 184.
[3] Charge-conjugate channels are implied throughout this Letter.
[4] T. Blake, G. Lanfranchi, and D. M. Straub, Prog. Part. Nucl. Phys. **92**, 50 (2017).
[5] S. Descotes-Genon, S. Fajfer, J. Kamenik, and M. Novoa-Brunet, Phys. Lett. B **809**, 135769 (2020).
[6] R. Aaij *et al.* (LHCb Collaboration), Phys. Rev. Lett. **122**, 191801 (2019).
[7] R. Aaij *et al.* (LHCb Collaboration), J. High Energy Phys. 08 (2017) 055.
[8] R. Aaij *et al.* (LHCb Collaboration), Phys. Rev. Lett. **111**, 191801 (2013).
[9] R. Aaij *et al.* (LHCb Collaboration), J. High Energy Phys. 06 (2014) 133.
[10] R. Aaij *et al.* (LHCb Collaboration), J. High Energy Phys. 02 (2016) 104.
[11] R. Aaij *et al.* (LHCb Collaboration), Phys. Rev. Lett. **125**, 011802 (2020).
[12] D. Bečirević, I. Doršner, S. Fajfer, D. A. Faroughy, N. Košnik, and O. Sumensari, Phys. Rev. D **98**, 055003 (2018).
[13] J. M. Camalich, M. Pospelov, P. N. H. Vuong, R. Ziegler, and J. Zupan, Phys. Rev. D **102**, 015023 (2020).
[14] A. Filimonova, R. Schäfer, and S. Westhoff, Phys. Rev. D **101**, 095006 (2020).
[15] T. E. Browder *et al.* (CLEO Collaboration), Phys. Rev. Lett. **86**, 2950 (2001).
[16] O. Lutz *et al.* (Belle Collaboration), Phys. Rev. D **87**, 111103 (2013).
[17] J. P. Lees *et al.* (*BABAR* Collaboration), Phys. Rev. D **87**, 112005 (2013).
[18] P. del Amo Sanchez *et al.* (*BABAR* Collaboration), Phys. Rev. D **82**, 112002 (2010).
[19] J. Grygier *et al.* (Belle Collaboration), Phys. Rev. D **96**, 091101 (2017); **97**, 099902(A) (2018).
[20] P. A. Zyla *et al.*, Prog. Theor. Exp. Phys. **2020**, 083C01 (2020).
[21] M. T. Prim, F. U. Bernlochner, P. Goldenzweig, M. Heck *et al.* (Belle Collaboration), Phys. Rev. D **101**, 032007 (2020).
[22] K. Akai, K. Furukawa, and H. Koiso (SuperKEKB Collaboration), Nucl. Instrum. Methods Phys. Res., Sect. A **907**, 188 (2018).
[23] F. Abudinén *et al.* (Belle II Collaboration), Chin. Phys. C **44**, 021001 (2020).
[24] B. Aubert *et al.* (*BABAR* Collaboration), Phys. Rev. D **72**, 032005 (2005).
[25] See Supplemental Material at http://link.aps.org/supplemental/10.1103/PhysRevLett.127.181802 for the list of the input variables used to train the classifiers; details about the event generators for simulation; the procedure followed to correct for the mismodeling of continuum events; additional figures presenting details about the fit, the limit setting, the signal efficiency and a comparison with previous results. The supplementary material includes Refs. [26–30].
[26] T. Fawcett, Pattern Recogn. Lett. **27**, 861 (2006).
[27] D. J. Lange, Nucl. Instrum. Methods Phys. Res., Sect. A **462**, 152 (2001).
[28] S. Jadach, B. F. L. Ward, and Z. Was, Comput. Phys. Commun. **130**, 260 (2000).
[29] T. Sjöstrand, S. Ask, J. R. Christiansen, R. Corke, N. Desai, P. Ilten, S. Mrenna, S. Prestel, C. O. Rasmussen, and P. Z. Skands, Comput. Phys. Commun. **191**, 159 (2015).
[30] S. Jadach, B. F. L. Ward, and Z. Was, Comput. Phys. Commun. **64**, 275 (1991).
[31] T. Kuhr, C. Pulvermacher, M. Ritter, T. Hauth, and N. Braun (Belle II Collaboration Framework Software Group), Comput. Software Big Sci. **3**, 1 (2019).
[32] S. Agostinelli *et al.* (GEANT4 Collaboration), Nucl. Instrum. Methods Phys. Res., Sect. A **506**, 250 (2003).
[33] T. Abe (Belle II Collaboration), arXiv:1011.0352.
[34] A. Abashian *et al.* (Belle Collaboration), Nucl. Instrum. Methods **479**, 117 (2002).
[35] E. Kou *et al.*, *The Belle II Physics Book* (Phys. Oxford University Press (OUP), Oxford, 2019), Vol. 2019, Chap. 5, pp. 57–61; Prog. Theor. Exp. Phys. **2020**, 029201(E) (2020).

[36] V. Bertacchi *et al.* (Belle II Tracking Group Collaboration), Comput. Phys. Commun. **259**, 107610 (2021).
[37] T. Keck, Comput. Software Big Sci. **1**, 2 (2017).
[38] A. J. Bevan *et al.*, *The Physics of the B Factories (Eur. Phys. J. C)* (Springer Publishing, New York, 2014), Vol. 74, Chap. 9.
[39] G. C. Fox and S. Wolfram, Nucl. Phys. **B149**, 413 (1979); **B157**, 543(E) (1979).
[40] S. H. Lee *et al.* (Belle Collaboration), Phys. Rev. Lett. **91**, 261801 (2003).
[41] D. Martschei, M. Feindt, S. Honc, and J. Wagner-Kuhr, J. Phys. Conf. Ser. **368**, 012028 (2012).
[42] J. L. Hodges, Arkiv för Matematik **3**, 469 (1958).
[43] L. Heinrich, M. Feickert, G. Stark, and K. Cranmer, J. Open Source Software **6**, 2823 (2021).
[44] L. Heinrich, M. Feickert, and G. Stark, PYHF: v0.5.4, https://github.com/scikit-hep/pyhf/releases/tag/v0.5.4.
[45] K. Cranmer *et al.* (ROOT Collaboration), Technical Report No. CERN-OPEN-2012-016, 2012.
[46] The product $\sigma_{\mathrm{BR}}\sqrt{L}$ of the total branching-fraction uncertainty σ_{BR} and the integrated luminosity of the data sample L is used as a measure, assuming that σ_{BR} scales as $1/\sqrt{L}$.
[47] A. L. Read, J. Phys. G **28**, 2693 (2002).
[48] G. Cowan, K. Cranmer, E. Gross, and O. Vitells, Eur. Phys. J. C **71**, 1554 (2011); **73**, 2501(E) (2013).